Signatures of van Hove Singularities Probed by the Supercurrent in a Graphene-hBN Superlattice

D. I. Indolese,[1,*] R. Delagrange,[1,†] P. Makk,[1,2] J. R. Wallbank,[3] K. Wanatabe,[4] T. Taniguchi,[4] and C. Schönenberger[1]
[1]Department of Physics, University of Basel, Klingelbergstrasse 82, CH-4056 Basel, Switzerland
[2]Department of Physics, Budapest University of Technology and Economics and Nanoelectronics Momentum Research Group of the Hungarian Academy of Sciences, Budafoki ut 8, 1111 Budapest, Hungary
[3]National Graphene Institute, University of Manchester, Manchester M13 9PL, United Kingdom
[4]National Institute for Material Science, 1-1 Namiki, Tsukuba 305-0044, Japan

(Received 28 May 2018; published 25 September 2018)

The band structure of graphene can be strongly modified if its lattice is aligned with the one of a boron nitride substrate. A moiré superlattice forms, which manifests itself by the appearance of new Dirac points, accompanied by van Hove singularities. In this work, we present supercurrent measurements in a Josephson junction made from such a graphene superlattice in the long and diffusive transport regime, where the critical current depends on the Thouless energy. We can then estimate the specific density of states of the graphene superlattice from the combined measurement of the critical current and the normal state resistance. The result matches with theoretical predictions and highlights the strong increase of the density of states at the van Hove singularities. By measuring the magnetic field dependence of the critical current, we find the presence of edge currents at these singularities. We explain it by the reduction of the Fermi velocity associated with the van Hove singularity, which suppresses the supercurrent in the bulk while the electrons at the edges remain less localized, resulting in an edge supercurrent. We attribute these different behaviors of the edges to defects or chemical doping.

DOI: 10.1103/PhysRevLett.121.137701

The combination of graphene with other 2D materials is a powerful means to engineer its electronic properties [1,2], for instance, by inducing spin-orbit coupling [3–8] or exchange interactions [9,10]. In particular, if graphene is placed on top of a hexagonal boron nitride (hBN) substrate, by aligning their crystallographic axes, a moiré superlattice is formed. This induces a periodic potential of wavelength λ of the order of 10 nm, leading to the modification of the band structure of graphene [11]. λ defines new Brillouin zone boundaries, where satellite Dirac points (SDPs) may appear [12,13]. In addition, van Hove singularities (VHSs) emerge in the density of states (DOS) at saddle points in the band structure due to the flattening of the arised minibands. These VHSs appear at a much lower energy than in standard graphene, where they are reachable only by chemical doping [14]. Because the DOS diverges and charge carriers of different sign coexist, a rich physics is expected, such as the formation of charge- or spin-density waves [15,16] or unconventional superconducting pairing mediated by electron-electron interaction [14]. Moreover, the Chern number is predicted to change from subband to subband [17], leading to valley Hall effect and topological edge current when the DOS is gapped at the main Dirac point (MDP) [18,19].

Graphene-hBN superlattices [1,2,20] and the induced VHSs [16,21,22] have been widely studied with normal metal leads, but only a few experiments have focused on the consequences of this rich physics for the Josephson effect. The investigation of the nondissipative current induced in a nonsuperconducting system using a Josephson junction (JJ) geometry is a powerful tool to investigate its physical properties, since the supercurrent is sensitive to the transport regime (ballistic or diffusive) [23–27], interactions [28,29], and the current distribution within the sample. For example, Josephson interferometry has been used recently to detect the presence of an edge current in quantum spin Hall systems [30,31] and in graphene, where an edge current was observed close to the Dirac point due to guided wave states [32] or, in bilayer graphene, due to the opening of a gap using an electric field [19]. In Ref. [19], an edge current in a graphene-hBN superlattice at the MDP is reported, where it is claimed that a gap opens due to sublattice symmetry breaking [2,33]. In contrast to these previous works, we investigate the supercurrent over the full range of energy, in order to probe the superlattice band structure.

We investigate the superconducting transport in long, diffusive JJs made from a graphene-hBN superlattice and show that the supercurrent carries in this transport regime the signature of its very specific band structure, in particular of the VHSs. First, by measuring both the normal state resistance R_N and the critical current I_c, we estimate the DOS of the JJs, which is then compared to theoretical calculations for a moiré superlattice. Furthermore, we extract the current distribution in the sample as a function of the charge carrier density from the magnetic field dependence of

I_c and show that edge currents appear at the VHSs, where the DOS diverges. We show that this edge current corresponds to a suppression of the supercurrent in the bulk, associated with the reduction of the Fermi velocity at the singularity that globally localizes the electrons. This suppression is not observed in the edges, probably because of edge defects or doping reduce the influence of the superlattice.

The measured sample is a hBN-graphene-hBN stack, where one hBN is aligned with the graphene. The heterostructure is contacted with superconducting edge contacts [34]. We fabricated the electrodes by cosputtering of MoRe (1:1) chosen for its large critical magnetic field (8 T) and high critical temperature (7 K) [35,36]. Several JJs are realized in the same stack with different lengths L from 0.45 to 1 μm and a width of $W = 3$ μm [Fig. 1(a)]. All measurements are performed in a dilution refrigerator at a base temperature of 70 mK.

Since the critical field of MoRe is too large to suppress the superconductivity by applying a magnetic field, we estimated the junction resistance R_N from the quasiparticle current measured when the JJ is voltage biased with $|eV| > 2\Delta_{\mathrm{MoRe}}$, with $\Delta_{\mathrm{MoRe}} = 1.3$ meV the superconducting gap of MoRe, estimated from multiple Andreev reflections [37]. The measurement is performed in a two-terminal configuration, such that R_N contains the resistance of the graphene channel R_G together with the contact resistance $2R_c$ ($R_N = R_G + 2R_c$).

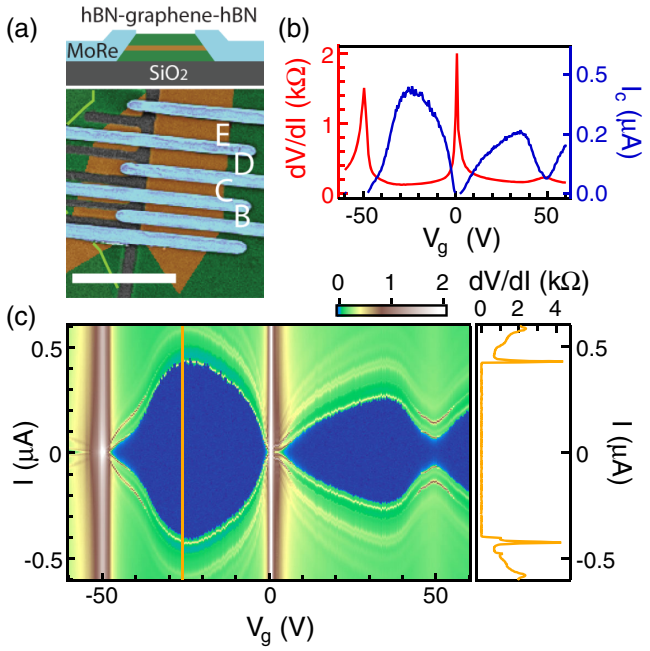

FIG. 1. (a) Top: Schematic side view of the device. Bottom: False-colored SEM image. The graphene (brown) is encapsulated between hBN (green) and contacted with MoRe (blue). The white scale bar corresponds to 5 μm. (b) Normal state resistance (red line) and critical current (blue line) as a function of gate voltage V_g for junction D. (c) Differential resistance as a function of V_g and dc current bias I for junction D. Right: Line cut at $V_g = -26$ V.

In the four junctions investigated, we observe an enhancement of resistance around the MDP ($V_g = 0$ V) and in addition around $V_g = \pm 50$ V, corresponding to a charge carrier density $n_0 = \pm 3.3 \times 10^{12}$ cm^{-2} [see Fig. 1(b)]. These additional resistance maxima are attributed to SDPs in the band structure and are clear evidence of a superlattice [1,33]. From n_0, we estimate the misalignment angle between the graphene and the hBN lattice to be around 0.7°. Note as well that no gap opening is observed at the MDP (Supplemental Material [37]). The analysis of the gate-dependent resistivity shows that all junctions are in the diffusive regime, where the mean free path is smaller than the junction length L.

We first measure I_c, defined as the maximal supercurrent that can be passed through the junction. To do so, we current bias the sample and measure the differential resistance as a function of bias current I and gate voltage (V_g) as shown in Fig. 1(c) for junction D (see Supplemental Material [37] for junctions B, C, and E). The switching from the zero resistance state to the normal resistance state is detected as a sharp transition at $I = I_c$, as presented in the right panel in Fig. 1(c) and plotted as a function of V_g in Fig. 1(b). No hysteresis was observed between the retrapping and switching current, indicating that the JJ is in the overdamped regime. At the first order, I_c is inversely proportional to R_N and is thus strongly reduced at the Dirac points, beyond the resolution of the measurement. I_c is globally smaller for electron doping ($V_g > 0$) than for hole doping. This reduction of I_c can be attributed to a p doping of the graphene by the MoRe, leading to the formation of a p-n junction between the metal contacts and n-doped graphene. Note that in previous works n doping of the contacts was observed [25,35]. This difference may be attributed to the work functions of graphene and MoRe, which are almost the same [47,48].

If the time τ spent by the electrons in the junction is short compared to $\hbar/\Delta$, in an ideal JJ, the product of R_N with I_c is expected to be proportional to the superconducting gap Δ [49]. But if τ exceeds $\hbar/\Delta$, then the relevant energy scale becomes the Thouless energy such that $eR_N I_c = \alpha E_{\mathrm{th}}$, with α a constant that depends on the transport regime (ballistic or diffusive) [23–25,50]. The four junctions we investigated are in this regime, since the superconducting coherence length $\xi_S < 200$ nm $< L$ [37]. In agreement with Refs. [23,24], we assume that the finite reflection probability at the contacts leads to an increase of τ such that it can be included as a reduction of α. Combining the expression of the Thouless energy $E_{\mathrm{th}} = \hbar D/L^2$ with the Einstein relation $L/WR_G = De^2 \times \mathrm{DOS}$, we find that the DOS as a function of the charge carrier density n can be determined from the measurement of both R_N and I_c:

$$\mathrm{DOS}(n) = \alpha \frac{\hbar}{R_N(n) R_G(n) e^3 L W I_c(n)}. \qquad (1)$$

Note that this formula involves R_G, which is obtained by subtracting the contact resistance R_c from the measured resistance R_N.

The DOS expected in the graphene-hBN superlattice was calculated using the methods described in Ref. [51]. The DOS on the hole side VHS is quite robust to small changes of the moiré parameters used in the theoretical model, while on the electron side it depends significantly on their choice. We chose here parameters similar to those extracted in Ref. [52], adapted to $\theta = 0.7°$, but slightly modified to produce a VHS on the electron side similar to previous measurements [13].

To compare our data with the theoretical calculated DOS, we have to make several assumptions: (i) The measurement of I_c is not affected by the finite temperature, (ii) the coefficient α is constant over the investigated gate range, and (iii) R_c is constant, respectively, for electron and hole doping. For the electronic temperature $T = 100$ mK, we estimate that hypothesis (i) is correct for measured critical currents higher than 30 nA [37], which excludes the gate regions around the MDP and the SDP at the hole side from the analysis. Concerning (ii), Refs. [23,24] have shown that α is indeed constant for a long diffusive graphene JJ, even if the measured value of 0.1–0.2 is substantially lower than the one expected for an ideal SNS junction [50]. (iii) is the strongest hypothesis, since R_c can actually depend on V_g and vary within a factor of 2 around the MDP [53,54], but we believe that even a gate-dependent contact resistance would not change the qualitative picture outlined below.

Then, by taking R_c and α as fitting parameters, we are able to reproduce the calculated DOS using Eq. (1) for $\alpha \in [0.3, 0.8]$ and $R_c \approx 40$–160Ω [37]. The result is plotted in Fig. 2. For the four junctions, this analysis matches qualitatively with the calculated DOS over a large gate range and reproduces well the VHSs. As theoretically expected, the superlattice features are less pronounced on the electron side. As a whole, despite some strong assumptions and some uncertainty in the precise value of the contact resistance, we show that the combined measurement of I_c and R_N allows us to estimate the DOS, providing information about the specific band structure of the superlattice. In particular, we see a clear signature of the VHSs, which was not explicitly present in either R_N or I_c.

It can be noted that the VHS at negative V_g is more pronounced for junctions B, C, and E than for junction D. In order to understand this discrepancy, we look now into the current distribution in junction D (see [37] for junction C) by measuring the interference pattern of I_c in a magnetic field [19,32].

Typical interference patterns are represented in Fig. 3(a) and compared to the Fraunhofer interference pattern, expected for a homogeneous current distribution [55] and a sinusoidal current phase relation as measured for graphene

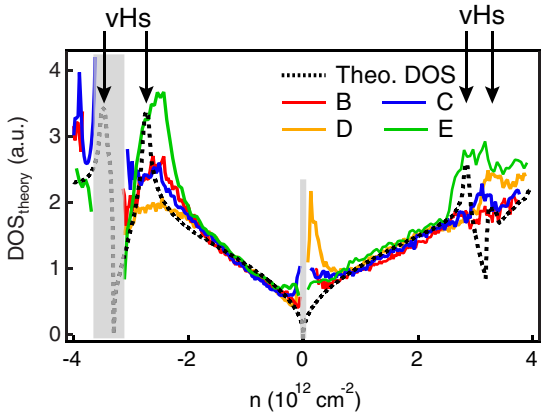

FIG. 2. Density of state estimated from measured R_N and I_c [Eq. (1)] (in red, blue, yellow, and green, respectively, for B, C, D, and E) compared to a calculation for $\theta = 0.7°$ (black line), as a function of the charge carrier density. The moiré superlattice parameters (defined in Ref. [52]) used to produce the theoretical DOS are $U_0^+ = 8.5$ meV, $U_1^+ = -8.5$ meV, and $U_3^+ = -14.7$ meV. The gray shaded areas correspond to regions where the critical current was too small to be measured.

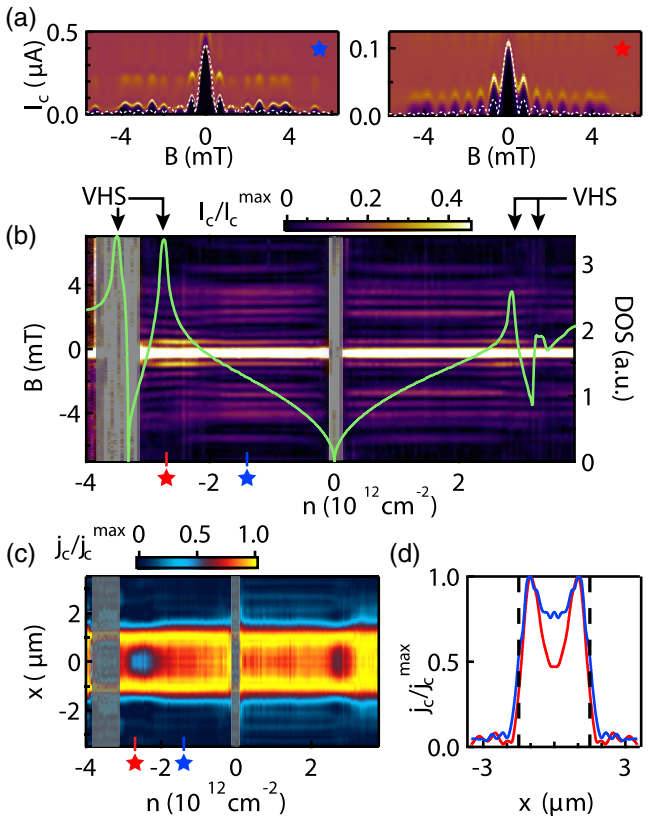

FIG. 3. (a) Differential resistance as a function of the current bias and magnetic field at $n_1 = -1.4 \times 10^{12}$ cm^{-2} (blue star) and $n_2 = -2.7 \times 10^{12}$ cm^{-2} (red star). White dashed line, expected Fraunhofer pattern for a homogeneous current density. (b) Normalized critical current as a function of magnetic field B and carrier density n measured in junction D, superimposed with the calculated DOS in green. (c) Calculated current density as a function of n and position along the contacts. (d) Line cuts of (c) at n_1 and n_2. The black dashed lines indicate the junction edges.

JJs [27,56]. At $V_g = -20$ V ($n_1 = -1.4 \times 10^{12}$ cm^{-2}), between the MDP and the VHS, the interference pattern matches a Fraunhofer pattern for the first few lobes, with a periodicity consistent with the junction dimensions taking the finite field penetration into the superconductor into account [32]. At slightly higher fields ($B > \pm 1.5$ mT), one can see some missing lobes and a nonvanishing supercurrent, indicating that the current is not perfectly homogeneous. The pattern at $V_g = -40$ V ($n_2 = -2.7 \times 10^{12}$ cm^{-2}), close to the VHS, is strikingly different, since the first lobes and the central peak are of comparable amplitude, which is an indication of an enhanced edge current [30].

In order to understand the gate dependence, we measure the interference pattern between $V_g = \pm 60$ V. We bias the sample with a linearly increasing current, at a rate of 0.17 A/s. I_c is obtained from the time at which the junction turns normal, averaged 200 times. The interference pattern can then be plotted as a function of the gate voltage [Fig. 3(b)]. In order to compare the shape of the interference patterns, for each V_g the critical current is normalized by its maximum value, $I_c(B = 0)$, for each gate voltage. Note that this kind of measurement cannot detect currents smaller than a few tens of nA, given by V_t/R_N with V_t the threshold voltage for the switching to a normal conducting state.

We can distinguish two different regimes for the interference pattern: Far from the VHSs, the interference pattern is gate independent and similar to the one described in Fig. 3(a), left. In contrast, around both VHSs, the pattern is similar to Fig. 3(b), right, where the side lobes become more prominent. The effect is stronger for hole doping, where the VHS is more pronounced.

To be more quantitative, we calculate the current distribution in the junction by the inverse Fourier transformation of the interference pattern for each V_g. The exact procedure is described in Supplement Material [37] and follows the ansatz given in Refs. [30,32]. The full map of the current density j_c as a function of V_g is shown in Fig. 3(c), where j_c was normalized by the maximal current density of each trace in n similar to Fig. 3(b). Two representative distributions are plotted in Fig. 3(d) for n_1 (blue line) and n_2 (red line), showing that in the whole junction the current partially accumulates on the edges and that the proportion of edge to bulk current is significantly larger at the VHS.

From the nonrenormalized map of the supercurrent distribution, we are able to extract separately the gate dependence of I_c on the edges of the junction (I_c^{edge}) and in the bulk (I_c^{bulk}) defined as shown in Fig. 4. In order to elucidate the nature of the edge current, we use the same procedure as for Fig. 2 to estimate the DOS of the bulk. For that, we use I_c^{bulk} instead of I_c and the same resistances R_N and R_c (assuming that the normal state resistance is dominated by the bulk). The result is shown in Fig. 4. We find a very good agreement between the DOS extracted from I_c^{bulk} (blue line) with the theoretically determined DOS (dotted line). In particular, the VHS is now better

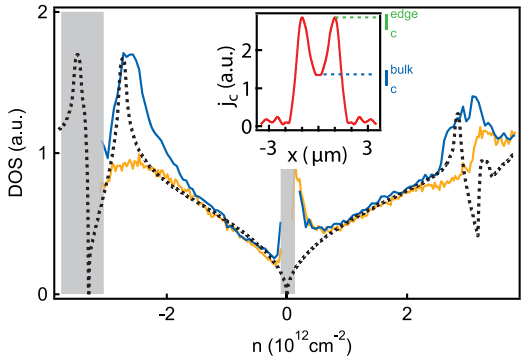

FIG. 4. DOS as a function of charge carrier density n in junction D, estimated from the bulk current (blue line; see inset) and the total current (yellow line). Inset: Current distribution at the VHS at a negative charge carrier density.

reproduced than using the total current I_c (plotted in yellow for comparison), meaning that the edge current does not carry the signature of the VHS. On the other hand, due to the flat band at the VHS, the Fermi velocity is expected to be globally reduced in the superlattice. This tends to localize the electron by increasing the traversal time τ of the electron in the junction and leads, therefore, to a reduction of the supercurrent. This localization acts weaker on the electrons at the edges, which leads to an increased edge to bulk current ratio at the VHS.

We performed the same measurement and data analysis for junction C [37]. There, the presence of an edge current is not observed as in junction D, and the DOS extracted using Eq. (1) exhibits a clear pronounced increase at the VHS. These two facts suggest that, in junction C, the edges are more affected by the superlattice potential than in junction D and show that both measurements of current distribution and DOS from R_N and I_c are consistent and complementary.

It remains to understand why the edges are behaving differently from the bulk in junction D. One can rule out the hypothesis of topological edges states due to the valley Hall effect at a gap opening (as proposed in Ref. [17] and measured in Ref. [18]), because the current at the edges appears far from any band crossing. It has been shown that an edge current can be induced as well by guided-wave electronic states due to the band bending at the sample edges [32] but only close to the Dirac point, where the edge potential is unscreened. Our measurement would be more consistent with previous works reporting an edge current induced by electrostatic or chemical doping of the edges [19,57–59]. This may induce disorder that can affect the superlattice potential such that the VHS may be smoothed [60]. This alteration could originate from the exposure of the graphene edge to ambient conditions during the fabrication or from contamination during the reactive ion etching used to shape the sample.

In conclusion, we demonstrate in this work that the supercurrent carries the signature of the graphene band

structure modified by the moiré superlattice. First, from the combined measurement of the normal resistance and the critical current and taking advantage of the diffusive regime, we estimate the DOS in the sample and find a very good qualitative agreement with the DOS calculated theoretically. In addition, Josephson interferometry reveals the presence of a gate-dependent edge current in junction D, and its proportion is strongly enhanced at the VHSs. By estimating the DOS for the bulk, we show that the edges are less affected by the superlattice potential, probably due to edge disorder or chemical doping. We then attribute the edge current to the lowering of the Fermi velocity in the bulk associated with the flat band at the VHS.

The authors thank C. Handschin and S. Zihlmann for their help in the lab and helpful discussions. We thank as well S. Goswami, Chuan Li, H. Bouchiat, S. Guéron, and V. Fal'ko for insightful discussions. This work has received funding from ERC project TopSupra (787414), the European Union Horizon 2020 research and innovation program under Grant Agreement No. 696656 (Graphene Flagship), the Swiss National Science Foundation, the Swiss Nanoscience Institute, and the Swiss NCCR QSIT, Topograph, ISpinText FlagERA network and from the OTKA PD-121052 and OTKA FK-123894 grants. P. M. acknowledges support from the Bolyai Fellowship. Growth of hexagonal boron nitride crystals was supported by the Elemental Strategy Initiative conducted by the MEXT, Japan and the CREST (JPMJCR15F3), JST. This research was supported by the National Research, Development and Innovation Fund of Hungary within the Quantum Technology National Excellence Program (Project No. 2017-1.2.1-NKP-2017-00001).

D. I. I. and R. D. contributed equally to this work.

*david.indolese@unibas.ch
†raphaelle.delagrange@unibas.ch

[1] L. A. Ponomarenko, R. V. Gorbachev, G. L. Yu, D. C. Elias, R. Jalil, A. A. Patel, A. Mishchenko, A. S. Mayorov, C. R. Woods, J. R. Wallbank, M. Mucha-Kruczynski, B. A. Piot, M. Potemski, I. V. Grigorieva, K. S. Novoselov, F. Guinea, V. I. Fal'ko, and A. K. Geim, Nature (London) **497**, 594 (2013).

[2] C. R. Woods, L. Britnell, A. Eckmann, R. S. Ma, J. C. Lu, H. M. Guo, X. Lin, G. L. Yu, Y. Cao, R. V. Gorbachev, A. V. Kretinin, J. Park, L. A. Ponomarenko, M. I. Katsnelson, Y. N. Gornostyrev, K. Watanabe, T. Taniguchi, C. Casiraghi, H. J. Gao, A. K. Geim, and K. S. Novoselov, Nat. Phys. **10**, 451 (2014).

[3] Z. Wang, D. K. Ki, H. Chen, H. Berger, A. H. MacDonald, and A. F. Morpurgo, Nat. Commun. **6**, 8339 (2015).

[4] Z. Wang, D. K. Ki, J. Y. Khoo, D. Mauro, H. Berger, L. S. Levitov, and A. F. Morpurgo, Phys. Rev. X **6**, 041020 (2016).

[5] B. Yang, M.-F. Tu, J. Kim, Y. Wu, H. Wang, J. Alicea, R. Wu, M. Bockrath, and J. Shi, 2D Mater. **3**, 031012 (2016).

[6] T. Völkl, T. Rockinger, M. Drienovsky, K. Watanabe, T. Taniguchi, D. Weiss, and J. Eroms, Phys. Rev. B **96**, 125405 (2017).

[7] S. Zihlmann, A. W. Cummings, J. H. Garcia, M. Kedves, K. Watanabe, T. Taniguchi, C. Schönenberger, and P. Makk, Phys. Rev. B **97**, 075434 (2018).

[8] T. Wakamura, F. Reale, P. Palczynski, S. Guéron, C. Mattevi, and H. Bouchiat, Phys. Rev. Lett. **120**, 106802 (2018).

[9] Z. Wang, C. Tang, R. Sachs, Y. Barlas, and J. Shi, Phys. Rev. Lett. **114**, 016603 (2015).

[10] J. C. Leutenantsmeyer, A. A. Kaverzin, M. Wojtaszek, and B. J. V. Wees, 2D Mater. **4**, 014001 (2017).

[11] M. Yankowitz, J. Xue, D. Cormode, J. D. Sanchez-Yamagishi, K. Watanabe, T. Taniguchi, P. Jarillo-Herrero, P. Jacquod, and B. J. LeRoy, Nat. Phys. **8**, 382 (2012).

[12] C. H. Park, L. Yang, Y. W. Son, M. L. Cohen, and S. G. Louie, Phys. Rev. Lett. **101**, 126804 (2008).

[13] G. L. Yu, R. V. Gorbachev, J. S. Tu, A. V. Kretinin, Y. Cao, R. Jalil, F. Withers, L. A. Ponomarenko, B. A. Piot, M. Potemski, D. C. Elias, X. Chen, K. Watanabe, T. Taniguchi, I. V. Grigorieva, K. S. Novoselov, V. I. Fal'ko, A. K. Geim, and A. Mishchenko, Nat. Phys. **10**, 525 (2014).

[14] J. L. McChesney, A. Bostwick, T. Ohta, T. Seyller, K. Horn, J. González, and E. Rotenberg, Phys. Rev. Lett. **104**, 136803 (2010).

[15] M. L. Kiesel, C. Platt, W. Hanke, D. A. Abanin, and R. Thomale, Phys. Rev. B **86**, 020507 (2012).

[16] G. Li, A. Luican, J. M. B. Lopes Dos Santos, A. H. Castro Neto, A. Reina, J. Kong, and E. Y. Andrei, Nat. Phys. **6**, 109 (2010).

[17] R. Brown, N. R. Walet, and F. Guinea, Phys. Rev. Lett. **120**, 026802 (2018).

[18] R. V. Gorbachev, J. C. W. Song, G. L. Yu, A. V. Kretinin, F. Withers, Y. Cao, A. Mishchenko, I. V. Grigorieva, K. S. Novoselov, L. S. Levitov, and A. K. Geim, Science **346**, 448 (2014).

[19] M. J. Zhu, A. V. Kretinin, M. D. Thompson, D. A. Bandurin, S. Hu, G. L. Yu, J. Birkbeck, A. Mishchenko, I. J. Vera-Marun, K. Watanabe, T. Taniguchi, M. Polini, J. R. Prance, K. S. Novoselov, A. K. Geim, and M. B. Shalom, Nat. Commun. **8**, 14552 (2016).

[20] C. Handschin, P. Makk, P. Rickhaus, M. H. Liu, K. Watanabe, T. Taniguchi, K. Richter, and C. Schönenberger, Nano Lett. **17**, 328 (2017).

[21] I. Brihuega, P. Mallet, H. González-Herrero, G. Trambly De Laissardière, M. M. Ugeda, L. Magaud, J. M. Gómez-Rodríguez, F. Ynduráin, and J. Y. Veuillen, Phys. Rev. Lett. **109**, 196802 (2012).

[22] Y. Kim, P. Herlinger, P. Moon, M. Koshino, T. Taniguchi, K. Watanabe, and J. H. Smet, Nano Lett. **16**, 5053 (2016).

[23] C. Li, S. Guéron, A. Chepelianskii, and H. Bouchiat, Phys. Rev. B **94**, 115405 (2016).

[24] C. T. Ke, I. V. Borzenets, A. W. Draelos, F. Amet, Y. Bomze, G. Jones, M. Craciun, S. Russo, M. Yamamoto, S. Tarucha, and G. Finkelstein, Nano Lett. **16**, 4788 (2016).

[25] I. V. Borzenets, F. Amet, C. T. Ke, A. W. Draelos, M. T. Wei, A. Seredinski, K. Watanabe, T. Taniguchi, Y. Bomze, M. Yamamoto, S. Tarucha, and G. Finkelstein, Phys. Rev. Lett. **117**, 237002 (2016).

[26] A. Murani, A. Kasumov, S. Sengupta, Y. A. Kasumov, V. T. Volkov, I. I. Khodos, F. Brisset, R. Delagrange, A. Chepelianskii, R. Deblock, H. Bouchiat, and S. Guéron, Nat. Commun. **8**, 15941 (2017).
[27] G. Nanda, J. L. Aguilera-Servin, P. Rakyta, A. Kormányos, R. Kleiner, D. Koelle, K. Watanabe, T. Taniguchi, L. M. Vandersypen, and S. Goswami, Nano Lett. **17**, 3396 (2017).
[28] J. A. Van Dam, Y. V. Nazarov, E. P. Bakkers, S. De Franceschi, and L. P. Kouwenhoven, Nature (London) **442**, 667 (2006).
[29] S. De Franceschi, L. Kouwenhoven, C. Schönenberger, and W. Wernsdorfer, Nat. Nanotechnol. **5**, 703 (2010).
[30] S. Hart, H. Ren, T. Wagner, P. Leubner, M. Mühlbauer, C. Brüne, H. Buhmann, L. W. Molenkamp, and A. Yacoby, Nat. Phys. **10**, 638 (2014).
[31] V. S. Pribiag, A. J. Beukman, F. Qu, M. C. Cassidy, C. Charpentier, W. Wegscheider, and L. P. Kouwenhoven, Nat. Nanotechnol. **10**, 593 (2015).
[32] M. T. Allen, O. Shtanko, I. C. Fulga, A. Akhmerov, K. Watanabi, T. Taniguchi, P. Jarillo-Herrero, L. S. Levitov, and A. Yacoby, Nat. Phys. **12**, 128 (2016).
[33] B. Hunt, J. D. Sanchez-Yamagishi, A. F. Young, M. Yankowitz, B. J. LeRoy, K. Watanabe, T. Taniguchi, P. Moon, M. Koshino, P. Jarillo-Herrero, and R. C. Ashoori, Science **340**, 1427 (2013).
[34] L. Wang, I. Meric, P. Y. Huang, Q. Gao, Y. Gao, H. Tran, T. Taniguchi, L. M. Campos, D. A. Muller, J. Guo, P. Kim, J. Hone, K. L. Shepard, and C. R. Dean, Science **342**, 614 (2013).
[35] V. E. Calado, S. Goswami, G. Nanda, M. Diez, A. R. Akhmerov, K. Watanabe, T. Taniguchi, T. M. Klapwijk, and L. M. K. Vandersypen, Nat. Nanotechnol. **10**, 761 (2015).
[36] F. Amet, C. T. Ke, I. V. Borzenets, Y.-M. Wang, K. Watanabe, T. Taniguchi, R. S. Deacon, M. Yamamoto, Y. Bomze, S. Tarucha, and G. Finkelstein, Science **352**, 966 (2016).
[37] See Supplemental Material at http://link.aps.org/supplemental/10.1103/PhysRevLett.121.137701 for details of device fabrication and measurement, additional data, and methods of the analysis, which includes Refs. [38–46].
[38] P. J. Zomer, M. H. D. Guimarães, J. C. Brant, N. Tombros, and B. J. Van Wees, Appl. Phys. Lett. **105**, 013101 (2014).
[39] D. A. Abanin and L. S. Levitov, Phys. Rev. B **78**, 035416 (2008).
[40] A. F. Young, C. R. Dean, L. Wang, H. Ren, P. Cadden-Zimansky, K. Watanabe, T. Taniguchi, J. Hone, K. L. Shepard, and P. Kim, Nat. Phys. **8**, 550 (2012).
[41] W. Yang, X. Lu, G. Chen, S. Wu, G. Xie, M. Cheng, D. Wang, R. Yang, D. Shi, K. Watanabe, T. Taniguchi, C. Voisin, B. Plaçais, Y. Zhang, and G. Zhang, Nano Lett. **16**, 2387 (2016).
[42] T. A. Fulton and L. N. Dunkleberger, Phys. Rev. B **9**, 4760 (1974).
[43] J. Clarke, A. N. Cleland, M. H. Devoret, D. Esteve, and J. M. Martinis, Science **239**, 992 (1988).
[44] M. H. Devoret, J. M. Martinis, and J. Clarke, Phys. Rev. Lett. **55**, 1908 (1985).
[45] I. V. Borzenets, Y. Shimazaki, G. F. Jones, M. F. Craciun, S. Russo, M. Yamamoto, and S. Tarucha, Sci. Rep. **6**, 23051 (2016).
[46] R. C. Dynes and T. A. Fulton, Phys. Rev. B **3**, 3015 (1971).
[47] Y.-J. Yu, Y. Zhao, S. Ryu, L. E. Brus, K. S. Kim, and P. Kim, Nano Lett. **9**, 3430 (2009).
[48] A. L. Smith, NASA technical report, 1970.
[49] M. Tinkham, *Introduction to Superconductivity* (McGraw-Hill, New York, 1996).
[50] P. Dubos, H. Courtois, B. Pannetier, F. K. Wilhelm, A. D. Zaikin, and G. Schön, Phys. Rev. B **63**, 064502 (2001).
[51] J. R. Wallbank, A. A. Patel, M. Mucha-Kruczyński, A. K. Geim, and V. I. Fal'ko, Phys. Rev. B **87**, 245408 (2013).
[52] M. Lee, J. R. Wallbank, P. Gallagher, K. Watanabe, T. Taniguchi, V. I. Fal'ko, and D. Goldhaber-Gordon, Science **353**, 1526 (2016).
[53] S. Russo, M. F. Craciun, M. Yamamoto, A. F. Morpurgo, and S. Tarucha, Physica E (Amsterdam) **42**, 677 (2010).
[54] F. Xia, V. Perebeinos, Y. M. Lin, Y. Wu, and P. Avouris, Nat. Nanotechnol. **6**, 179 (2011).
[55] J. C. Cuevas and F. S. Bergeret, Phys. Rev. Lett. **99**, 217002 (2007).
[56] L. Bretheau, J. I. -J. Wang, R. Pisoni, K. Watanabe, T. Taniguchi, and P. Jarillo-Herrero, Nat. Phys. **13**, 756 (2017).
[57] Z. Dou, S. Morikawa, A. Cresti, S. W. Wang, C. G. Smith, C. Melios, O. Kazakova, K. Watanabe, T. Taniguchi, S. Masubuchi, T. Machida, and M. R. Connolly, Nano Lett. **18**, 2530 (2018).
[58] A. Woessner, P. Alonso-González, M. B. Lundeberg, Y. Gao, J. E. Barrios-Vargas, G. Navickaite, Q. Ma, D. Janner, K. Watanabe, A. W. Cummings, T. Taniguchi, V. Pruneri, S. Roche, P. Jarillo-Herrero, J. Hone, R. Hillenbrand, and F. H. Koppens, Nat. Commun. **7**, 10783 (2016).
[59] V. Panchal, A. Lartsev, A. Manzin, R. Yakimova, A. Tzalenchuk, and O. Kazakova, Sci. Rep. **4**, 5881 (2014).
[60] A. Lherbier, B. Biel, Y. M. Niquet, and S. Roche, Phys. Rev. Lett. **100**, 036803 (2008).